Modeling Marine Stratocumulus with a Detailed Microphysical Scheme

ZHAO Chunsheng*[1] (赵春生), and Yutaka ISHIZAKA

[1]*Department of Atmospheric Science, School of Physics, Peking University, Beijing* 100871

[2]*HyARC, Nagoya University, Nagoya, Japan*

(Received 29 January 2003; revised 23 April 2003)

ABSTRACT

A one-dimensional 3rd-order turbulence closure model with size-resolved microphysics and radiative transfer has been developed for investigating aerosol and cloud interactions of the stratocumulus-topped marine boundary layer. A new method is presented for coupling between the dynamical model and the microphysical model. This scheme allows the liquid water related correlations to be directly calculated rather than parameterized. On 21 April 2001, a marine stratocumulus was observed by the Caesar aircraft over the west Pacific Rim south of Japan during the 2001 APEX/ACE-Asia field measurements. This cloud is simulated by the model we present here. The model results show that the general features of the stratocumulus-topped marine boundary layer predicted by the model are in agreement with the measurements. A new onboard cloud condensation nuclei (CCN) counter provides not only total CCN number concentration (as the traditional CCN counters do at a certain supersaturation) but also the CCN size distribution information. Using these CCN data, model responses to different CCN initial concentrations are examined. The model results are consistent with both observations and expectations. The numerical results show that the cloud microphysical properties are changed fundamentally by different initial CCN concentrations but the cloud liquid water content does not differ significantly. Different initial CCN loadings have large impacts on the evolution of cloud microstructure and radiation transfer while they have a modest effect on thermodynamics. Increased CCN concentration leads to significant decrease of cloud effective radius.

Key words: cloud condensation nuclei, aerosol, cloud, marine stratocumulus, modeling

1. Introduction

Stratocumulus clouds occur frequently over large areas of the world, especially over the sea. Marine stratocumuli are known to play an important role in the global radiation budget, and consequently the earth's climate. Since boundary layer clouds generally have high albedo, these clouds significantly decrease the amount of solar energy absorbed by the earth system, reducing heating rates as compared to cloud-free conditions (Nicholls, 1984; Randall et al., 1984). Twomey et al. (1977, 1974) demonstrated that the reflectivity of water clouds with modest optical depths increases as the abundance of cloud condensation nuclei (CCN) increases. This indirect forcing of aerosols is likely to counteract part of the warming due to greenhouse gases (Slingo, 1990) and dependencies are sensitive to small changes in the characterization of stratiform clouds. The impact of boundary layer stratus on the radiation budget and the amounts of energy that they absorb depends upon both the microphysical and macrophysical properties of these clouds.

Therefore, the accurate determination of the microphysical (e.g., cloud droplet size) and macrophysical (e.g., cloud area extent) properties of boundary layer stratus is essential for the correct treatment of these clouds in radiative transfer and global climate models. Moreover, since cloud absorption is dependent upon the spatial distribution and sizes of the cloud droplets, understanding the detailed microphysical processes in boundary layer stratus requires knowledge of the CCN, cloud dynamics, cloud microphysics, turbulence, and radiation interactions. In order to simulate such a complex system of mutual interactions, it is crucial to develop a detailed microphysical model to describe the aerosol and cloud processes.

*E-mail: zcs@pku.edu.cn

There are a number of models developed with a varying complexity to study different aspects of a marine stratocumulus-topped boundary. They range from mixed-layer models with bulk water schemes to LES (Large Eddy Simulation) models with explicit microphysics. The most fundamental simulations can be obtained by LES. Unfortunately LES is extremely CPU expensive and is, as yet, prohibitive for extensive simulations of microphysics and especially unpractical for studying aerosol-cloud interactions on timescales of days.

Bechtold et al. (1996) carried out intercomparison studies among different one-dimensional codes and with LES on modeling a stratocumulus-topped PBL. It is shown that 1D models can reasonably represent the main features (cloud water content, cloud fraction, and some turbulence statistics) of a well-mixed stratocumulus-topped boundary layer. Bougeault (1985) presented results of a 3rd-order turbulence closure model for a run of 7 days, which showed features very similar to those observed (Nicholls, 1984). Duynkerke and Driedonks (1987) showed results of a higher-order closure model that compares favorably with different types of experiments.

Higher-order closure models seem to be able to describe a great variety of phenomena in the cloud-topped marine boundary layer than the mixed-layer models since the well-mixed assumption is often too strong. Due to their flexibility, higher-order closure models allow for the decoupling between the cloud layer and sub-cloud layer (Bougeault, 1985; Duynkerke and Driedonks, 1987), and they can simulate both shear and buoyancy production and its influence on the entrainment rate (Duynkerke and Driedonks, 1988). Higher-order turbulence closure models represent a balance between physical sophistication and computational expense compared with simple mixed-layer models (Lilly, 1968) and sophisticated large-eddy simulation (LES) models (Moeng, 1986). Although there are some fundamental drawbacks of one-dimensional models as discussed in Brown (1997) and Stevens (Stevens et al., 1998), a one-dimensional high-order closure model with detailed cloud microphysics is still an attractive tool for studying the interactions between dynamics, cloud physics, and radiation processes.

Changes in aerosol properties caused by pollution can affect the radiative balance of the Earth by influencing the properties of clouds. The magnitude of this aerosol, indirect effect depends on the number of aerosols and the physical-chemical properties of the individual aerosol particles comprising the aerosol size distribution as well as on the type of clouds involved. The size distribution of water drops has a great impact on cloud radiation processes, and therefore can greatly influence the turbulent structure and dynamics within clouds. Also the size distribution and chemical composition of aerosols are critical for CCN activation.

Studies have dealt with several aspects of the overall problem and have ranged in scope from theoretical studies to formulate the equations that govern the physical processes of concern to large field experiments that collect descriptions of the dynamical and microphysical conditions which prevail in actual clouds.

In the past few years, a number of studies have been carried out with a higher order-turbulence closure model coupled to a sectional representation of cloud microphysics (Ackerman et al., 1995; Bott et al., 1996). These models were widely applied to investigate aerosol emission perturbations by ship track (Taylor and Ackerman, 1999), cloud, radiation, and chemical processes in marine stratus (Bott, 1998, 1999). Unfortunately, in their models, the liquid water related correlations are obtained by the condensation parameterization schemes (Sommeria and Deardorff, 1977; Mellor, 1977; Bougeault, 1981a, b). Actually the liquid water content related correlations can also be derived from the size-resolved particles related correlations. The size-resolved particle number concentration related correlations can be resolved using the high-order turbulence closure method. A new coupling method to directly calculate the liquid water related correlations is developed in this model. The high-order turbulent closure scheme provides us a platform to calculate these microphysical related correlations.

The objectives of the paper are (1) to present a one-dimensional 3rd-order turbulence closure model with explicit microphysics and a new method of coupling between the one-dimensional dynamical model and the explicit microphysical model; (2) to apply the model in a simulation of a stratocumulus cloud case of 21 April 2001 from 2001 APEX (Asian Atmospheric Particulate Environment Change Studies) /ACE-Asia (Asian Pacific Regional Aerosol Characterization Experiment) field measurements; and (3) to conduct sensitivities studies based on aircraft observational data to investigate the effects of different CCN concentrations on dynamics, microphysics, and radiation of a stratocumulus-topped boundary layer.

2. Model description

We have developed a one-dimensional high-order turbulent closure model to represent the stratocumulus-topped marine boundary layer. The model is composed of a one-dimensional third-order turbulence closure model, a radiation model, and a size-resolved microphysical model. A new method for calculating the water related correlations is used in the

coupling between the dynamical model and the microphysical model.

2.1 *Dynamic framework*

The 3rd-order turbulence closure model used in this model closely follows that of Bougeault (1981a, b) except for the liquid water related statistics. Wang and Wang (1994) studied the effects of drizzle on a cloud-topped marine boundary layer using the similar turbulence closure model. The model uses the conservative variable $\theta_{\rm l}$ (liquid water potential temperature) and $q_{\rm t}$ (total water content) to describe the thermodynamic properties of the cloudy boundary layer. The liquid water content is predicted directly from water drop size distribution of the detailed microphysical model. The values of the mean potential temperature θ and water vapor content $q_{\rm v}$ can be derived from

$$\overline{\theta} = \overline{\theta_{\rm l}} + \left[\frac{p_0}{p(z)}\right]^k \frac{L}{c_p}\overline{q_{\rm l}}\,, \tag{1}$$

$$\overline{q_{\rm v}} = \overline{q_{\rm t}} - \overline{q_{\rm l}}\,, \tag{2}$$

where L is the latent heat of vaporization of water, c_p the specific heat of constant pressure for moist air, p_0 the surface pressure, $p(z)$ the pressure at height z, $q_{\rm v}$ the water vapor mixing ratio, $q_{\rm l}$ the liquid water content, and $q_{\rm t}$ the total water mixing ratio.

2.2 *Aerosol and cloud microphysical model*

A spatially homogeneous aerosol undergoing nucleation, condensation, and coagulation is simulated by numerical solution of the general dynamic equation (GDE). A particularly powerful technique for solving GDE is the so-called sectional method or bin model. In this discrete approach to modeling aerosol dynamics, the aerosol size range is divided into a number of sections. Approximating the mass, number, or surface area distribution function as a constant within each section results in a set of differential equations for the properties of each section.

The size-resolved aerosol model used in this paper was originally developed by Zhao (1996, 1998) to study aerosol size formation and evolution processes in the remote marine boundary layer. It has since been improved and implemented to simulate the aerosol and cloud microphysical processes. Here, only a general description of the overall characteristics of the model is given. A more detailed description is given for the coupling between the dynamic model and the microphysical model.

The particle size distributions for aerosol and droplets are each divided into 20 bins with geometrically increasing size, such that the particle volume doubles between successive bins, resulting in a diameter grid that spans from a minimum of 0.005 μm to a maximum of 41 μm. Within each droplet size bin, the model solves a continuity equation for the total volume concentration of dissolved cloud condensation nuclei to allow calculation of equilibrium reduction in droplet vapor pressure (the solute effect).

The liquid water spectrum is represented by $n(r)dr$ which is the number of droplets per unit volume between the radius r and $r+\delta r$. The analytical form of the equation governing the time rate of change of the one-dimensional number density function due to the processes of nucleation, condensation, coalescence, advection, and sedimentation is

$$\begin{aligned}\frac{\partial n_i}{\partial t} = &-\frac{\partial}{\partial z}(wn_i) - w\frac{\partial n_i}{\partial z} + S - R - \frac{\partial}{\partial m_i}(g_m n_i)\\ &+ \int_{r_{\min}}^{r} n(r')n(r-r')K_1 dr'\\ &- \int_{r_{\min}}^{r_{\max}} n(r)n(r')K_2 dr'\,,\end{aligned} \tag{3}$$

where the first and second terms on the right-hand side account for the transport and sedimentation of different size particles respectively. The third and forth terms are the source and sink terms. The fifth term is the condensation growth term of cloud drops. The last two terms are the coagulation/coalescence terms which represent different collision mechanisms by different coagulation kernels. The physical descriptions of each of the terms of the above equation are presented below.

2.3 *CCN activation*

In this model, supersaturation is explicitly calculated by water vapor concentration and temperature at each time step and each spatial point. This explicit treatment of supersaturation requires a small time step to avoid numerical instabilities. Here a variable time step method is used. The dry particles in a size bin are activated to CCN as soon as supersaturation exceeds their critical supersaturation. The maximum value of supersaturation for which a droplet can maintain stable equilibrium with respect to condensation is determined by a simplified form of the Kohler equilibrium relations (Pruppacher and Klett, 1997):

$$\frac{e_{\rm a}}{e_{\rm sat,w}} = \exp\left[\frac{2M_{\rm w}\delta_{\rm s/a}}{RT\rho_{\rm w}r} - \frac{\gamma\Phi_{\rm s}m_{\rm s}M_{\rm w}/M_{\rm s}}{(4\pi r^3\rho_{\rm s}''/3) - m_{\rm s}}\right]\,, \tag{4}$$

where $e_{\rm a}$ is saturation vapor pressure in the environment at the drop surface, $e_{\rm sat,w}$ saturation vapor pressure over water, $M_{\rm w}$ molecular weight of water, $M_{\rm s}$ molecular weight of salt, $\sigma_{\rm s/a}$ surface tension of solution against air, $\rho_{\rm w}$ density of water, r radius of drop, γ number of ions into which a salt molecule dissociates in water, $\Phi_{\rm s}$ osmotic coefficient, $m_{\rm s}$ mass of salt

particle, and ρ_s density of aqueous salt solution. Saturation vapor pressure $e_{sat,w}$ in bars over liquid water are from Buck (1981):

$$e_{sat,w} = 6.1121 \times 10^3 \frac{\exp(18.729 - \frac{T}{227.3})T}{257.87 + T}, \quad (5)$$

in which T is air temperature in °C. Errors in estimates of saturation vapor pressure over water for the range –40°C to +50°C are less than deviations caused by temperature measurement errors of 0.23°C.

2.4 *Condensation/evaporation*

The numerical approach for this process is the same as in the work of Zhao (1996, 1998). Only a brief description of this process is made here. The rate of growth of cloud droplets is determined by considering the simultaneous quasi-steady diffusion transport of mass and latent heat from a falling water droplet. Once cloud nuclei are activated, their further growth is governed by the droplet condensational growth equation which is taken in the form similar to that employed by Barkstrom (1978):

$$\frac{dm}{dt} = \frac{(4\pi r f_2 k_1)[(S-1) - \frac{2S}{\rho_L R_w T_r} + \phi]}{\left[\frac{L^2}{R_w T^2} + \left(\frac{f_2 k_1}{f_1 D}\right)\left(\frac{R_w T}{e_s}\right)\right]}, \quad (6)$$

where S is supersaturation which is calculated by water vapor concentration and temperature at each time step, e_s saturation vapor pressure, k_1 diffusion coefficient for heat in air, f_1 and f_2 correction for the kinetic behavior of water molecules, ρ_L mass density of liquid water, D diffusion coefficient for water vapor, and ϕ correction function for concentration.

2.5 *Coagulation and coalescence*

Coagulation and coalescence may be driven by any process that is able to force two or more particles together, whether Brownian diffusion, gravitational settling, shear flow, or any of a number of other mechanisms. In the atmosphere, Brownian coagulation tends to dominate under most circumstances and sedimentation-driven forms are generally significant only for particles greater than a few microns in radius. In this model, both Brownian coagulation and gravitational collection are taken into account by the coagulation kernels similar to Hall (1980) and Zhao (1998). The numerical treatment of coagulation is based on the method of Zhao (1998).

2.6 *Sedimentation*

Although gradational settling is only significant for the largest of the aerosol particles, it is noteworthy in that this is the one process for which a general representation is reasonably well defined. As pointed out by Feingold et al. (1996), the sedimentation process is also important if one is to represent drizzling boundary layers with integrity. Sensitivities studies of Feingold et al. (1998) showed that sedimentation plays an important role in stratocumulus that requires more accurate treatment than a simple sedimentation of all drops at mass-mean velocity. In this model, each particle falls at its own terminal velocity and the corresponding equations follow those of Pruppacher and Klett (1997).

3. Radiative transfer model

The object of the atmospheric radiative transfer model is to provide a simple, accurate, and fast method of calculating the total radiative flux profile within the atmosphere. These calculations supply the vertical and horizontal radiative flux divergence to calculate the radiative heating and cooling rates.

It is necessary to parameterize the emissivity of gases and water drops in order to simulate longwave and shortwave radiation. Here only an overview is presented, since the details of the techniques can be referred to in other places (Liou, 1992; Liou et al., 1998; Ding, 2001). The model treats multiple scattering over 18 wavelengths. The upward and downward radiative fluxes at each layer are calculated using the δ–4 stream method (Liou, 1992). Gases of CO_2, CH_4, and N_2O are assumed to be mixed uniformly through the atmosphere with concentrations of 330, 1.6, and 0.28 ppmv. The ozone profile is taken from the U.S. Standard Atmosphere (NOAA, 1976).

4. A new coupling method

The liquid water content q_l can be calculated from the predicted water drop concentration in each bin by the explicit microphysical model.

$$q_l(z) = \sum_{i=1}^{T_n} \frac{4}{3}\pi r_i^3 \rho_w \overline{n_i}(z), \quad (7)$$

where T_n is the total bin number of cloud drops, r_i is the mean radius of the ith bin particles, and ρ_w is the water droplet density.

The high order turbulence closure model provides a consistent scheme for all the scalar variables (Bougeault, 1981a, b). We assume the particle number concentration of each bin is a scalar variable just like other scalar variables such as temperature. Using the same closure scheme as temperature, we can calculate all the 2-moment ($\overline{a'n_i'}$) and 3-moment ($\overline{a'b'n_i'}$)

correlations of n_i', where a and b appearing in $\overline{a'n_i'}$ and $\overline{a'b'n_i'}$ represent any of θ_l, q_t, u, v, and w. For instance, for the 2-moment correlations $\overline{a'n_i'}$, they are $\overline{w'n_i'}, \overline{u'n_i'}, \overline{v'n_i'}, \overline{n_i'n_i'}, \overline{q_t'n_i'}, \overline{\theta_l'n_i'}$. The corresponding to equations for solving these correlations can be referred in Bougeault (1981a, b). As an example, the following are the equations for $\overline{w'n_i'}$.

$$\frac{\partial}{\partial t}\overline{w'n_i'} = -\frac{\partial}{\partial z}\overline{w'w'n_i'} - \overline{w'w'}\frac{\partial \overline{n_i}}{\partial z} - (1-C_7)\left(\overline{w'n_i'}\frac{\partial \overline{w}}{\partial z} - \beta\overline{\theta_v'n_i'}\right) - \frac{C_6}{\tau}\overline{w'n_i'}\,, \quad (8)$$

$$\frac{\partial}{\partial t}\overline{n_i'n_j'} = -\frac{\partial}{\partial z}\overline{w'n_i'n_j'} - \left(\overline{w'n_j'}\frac{\partial \overline{n_i'}}{\partial z} + \overline{w'n_i'}\frac{\partial \overline{n_j'}}{\partial z}\right) - \frac{C_6}{\tau}\overline{n_i'n_j'}\,, \quad (9)$$

$$\frac{\partial}{\partial t}\overline{w'w'n_i'} = -\overline{w'n_i'}\frac{\partial \overline{w'w'}}{\partial z} - 2\overline{w'w'}\frac{\partial \overline{w'n_i'}}{\partial z} - \overline{w'w'w'}\frac{\partial \overline{n_i}}{\partial z} + \left(-2\overline{w'w'n_i'}\frac{\partial \overline{w}}{\partial z} - 2\beta\overline{w'\theta_v'n_i'}\right)(1-C_{11}) - \frac{C_8}{\tau}\overline{w'w'n_i'}\,, \quad (10)$$

$$\frac{\partial}{\partial t}\overline{w'n_i'n_j'} = -\overline{w'w'}\frac{\partial \overline{n_i'n_j'}}{\partial z} - \overline{w'n_i'}\frac{\partial \overline{w'n_j'}}{\partial z} - \overline{w'n_j'}\frac{\partial \overline{w'n_i'}}{\partial z} - \overline{w'n_i'n_j'}\frac{\partial \overline{n_j}}{\partial z} - \overline{w'w'n_i'}\frac{\partial \overline{n_j}}{\partial z} - \overline{w'w'n_j'}\frac{\partial \overline{n_i}}{\partial z} + \left(-\overline{w'n_i'n_j'}\frac{\partial \overline{w}}{\partial z} + \beta\overline{\theta_v'n_i'n_j'}\right)(1-C_{11}) - \frac{C_8}{\tau}\overline{w'n_i'n_j'}\,. \quad (11)$$

The coefficients and constants appearing in the above equations are same as those used by Bougeault (1981a, b).

Traditionally, the liquid water related correlations are obtained by the condensation parameterization schemes (Sommeria and Deardorff, 1977; Mellor, 1977; Bougeault, 1981a, b). Ackerman et al. (1995) used the Bougeault method for their bouyancy flux treatment in their high-order turbulence closure model with explicit microphysics. As we mentioned above, the size-resolved particle number concentration related correlations can be resolved using the turbulence closure scheme. Therefore, the liquid water content related correlations can also be derived from the n_i' related correlations. Liquid water related fluxes ($\overline{a'q_l'}$) are calculated by summing up all the water drops fluxes ($\overline{a'n(i)'}$). It is assumed here that an italic represents any of θ_l, q_t, u, v and w, which are $\overline{w'\theta_v'}$, $\overline{u'\theta_v'}$, $\overline{v'\theta_v'}$, $\overline{\theta_v'\theta_v'}$, $\overline{q_t'\theta_v'}$, and $\overline{\theta_l'\theta_v'}$. Taking liquid water flux ($\overline{w'q_l'}$) as an example, it is calculated as follows:

$$\overline{w'q_l'} = \sum_i^{n_{bin}} \frac{4}{3}\pi r_i^3 \rho_w \overline{w'n_i'}\,. \quad (12)$$

Whenever the virtual potential temperature θ_v appears, it is expressed as follows (Bougeault, 1981a, b):

$$\overline{\theta_v} = \overline{\theta_l} + 0.61T_0\overline{q_t} + \left[\left(\frac{p_0}{p_r(z)}\right)^k \frac{L}{c_p} - 1.61T_0\right]\overline{q_l'}\,, \quad (13)$$

where T_0 is a mean value of the absolute temperature, L the latent heat of the condensation of water, c_p the specific heat for moist air, p_0 the reference pressure 1000 hPa, and $p_r(z)$ the mean pressure of the Boussinesq reference atmosphere at height z.

The correlations arising from the buoyancy terms $\beta\overline{a'\theta_v'}$ and $\beta\overline{a'b'\theta_v'}$, are calculated using the predicted correlations of $\overline{a'\theta_l'}, \overline{a'q_w'}$, and $\overline{a'q_l'}$. As an example, the buoyancy flux ($\overline{w'\theta_v'}$) is computed using the predicted variables $\overline{w'\theta_l'}, \overline{w'q_w'}$, and $\overline{w'q_l'}(\overline{w'n_i'})$, namely as

$$\overline{w'\theta_v'} = \overline{w'\theta_l'} + 0.61T_0\overline{w'q_t'} + \left[\left(\frac{p_0}{p_r(z)}\right)^k \frac{L}{c_p} - 1.61T_0\right]\overline{w'q_l'}\,. \quad (14)$$

The main concept behind this coupling method is that not only the aerosol and cloud number concentrations are size-resolved but also their 2-moment and 3-moment correlations of different particles. Using the same turbulence closure scheme, the size-resolving particle related correlations can be computed explicitly. All macro-properties of cloud as cloud liquid water related variables (mean and correlations) are calculated from the sized-resolved microphysical variables directly with the same closure scheme. The advantage is that such a direct calculation of all particle correlations is physically consistent in the high-order turbulence closure model. The disadvantage is that additional equations appear and this therefore increases the expense of the calculations.

5. Model initialization

In simulating the marine stratocumulus, Duynkerke and Driedonks (1987) initialized their model with the observed cloud structure and compared their model

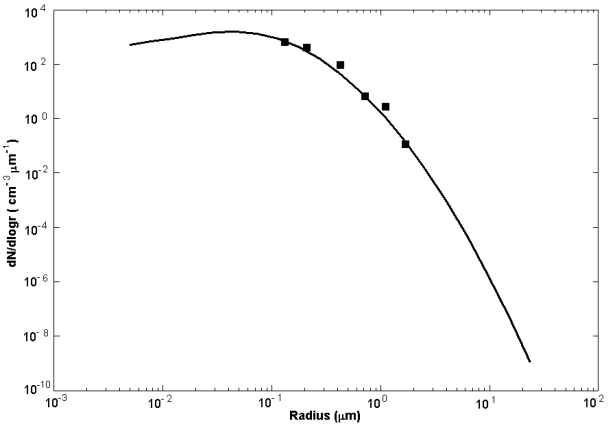

Fig. 1. The initial size distribution for dry particles based on the fitting of CCN measurement data. Square marks are the aircraft CCN data of 21 April 2001. The line is the lognormal fitting result.

results with the measurements after 2 hours of simulation time. Bougeault (1985) initialized his model with a cloud-free, stable atmosphere, simulating 7 days of evolution; the results on noon of the fourth day when steady state was reached were compared with the measurements. Ackerman et al. (1995) took an intermediate approach by initializing their model with a cloudless, slightly unstable boundary layer at midnight and comparing the model results 12 hours later with the measurements. Here we take a similar approach to Ackerman et al. (1995). The model run is started at local midnight 20 April 2001. The model results and measurements are compared after 10 hours of simulation.

The aircraft measurements of aerosol and cloud properties were undertaken over the west Pacific on 21 April 2001. Measurements illustrated the presence of a well mixed boundary layer with a solid, nonprecipitating, stratocumulus cloud deck. During this flight, aerosol measurements were taken below, in, and above the cloud. The initial sounding used in our model is loosely based on the measurements. The sea surface temperature is 288 K. The dry potential temperature profile is slightly stable in the PBL and increases from 288 K at the surface to 288.32 K at the inversion base at 690 m, and then rapidly increases to a value of 294.4 K at the inversion top at 785 m. The total water mixing ratio (water vapor plus liquid water) is constant in the PBL, with a value of 8.1 g kg^{-1}, and decreases to a value of 4.6 g kg^{-1} throughout the inversion. The surface mixing ratio is set equal to the saturation mixing ratio. A divergence of 5.6×10^{-5} s^{-1} is applied to limit the rise of the mean cloud top. The vertical grid spacing is 20 m. The dynamical timestep is 4 seconds and the radiation scheme is called every 2 minutes. A variable time step for microphysical calculation is used to avoid numerical instabilities.

The crucial problem in driving the model is the determination of the initial aerosol size distribution. The particle size distribution was measured by onboard instruments of a new CCN counter and (Aoctive Scattering Aerosol Spectrometer Probe). This new CCN counter (Model ACN-1000, SIGMATEC) designed by Dr. Ishizaka, Nagoya University, has 4 channels with controllable supersaturation. Unlike the traditional CCN counters, it provides not only the total CCN number concentration at certain supersaturations but also the size spectrum of the CCN.

In utilizing the CCN data, we perform a lognormal size distribution fitting to the particle number distributions. Lognormal distributions represent many of the distributions actually recorded by the in situ probes and are frequently used in cloud and radiation studies (Seinfeld and Pandis, 1998; Pruppacher and Klett, 1997). In order to obtain the dry CN size distribution, the observed CCN spectrum is converted into a dry particle size distribution at 99% relative humidity with the Kohler equation. The parameters of the lognormal distribution are calculated with the following equations as we fit a lognormal distribution to the converted dry particle size distribution:

$$R_{\rm n} = \exp\left\{\frac{\sum_{i=1}^{N_{\rm bins}} n(i)\cdot\lg(r_i)}{\sum_{i=1}^{N_{\rm bins}} n(i)}\right\}, \tag{15}$$

$$\sigma = \exp\left\{\left[\frac{\sum_{i=1}^{N_{\rm bins}} n(i)\cdot(\lg(r_i)-\lg(R))^2}{\sum_{i=1}^{N_{\rm bins}} n(i)}\right]^{1/2}\right\}, \tag{16}$$

where $R_{\rm n}$ is the geometric mean number radius, σ is the geometric standard deviation, and $n(i)$ the particle number concentration at each size range.

The same method is used for ASASP data to cover the size range smaller than 0.1 μm. Thus two lognormal size distributions based on measurement data are used to describe the initialization of the microphysical model:

$$\frac{dN(r)}{d(\lg r)} = \sum_{i=1}^{2}\frac{n_{\rm t}}{(2\pi)^{1/2}\lg\sigma_i}\exp\left\{-\frac{\left[\lg\left(\frac{r}{R}\right)\right]^2}{2(\lg\sigma_i)^2}\right\}, \tag{17}$$

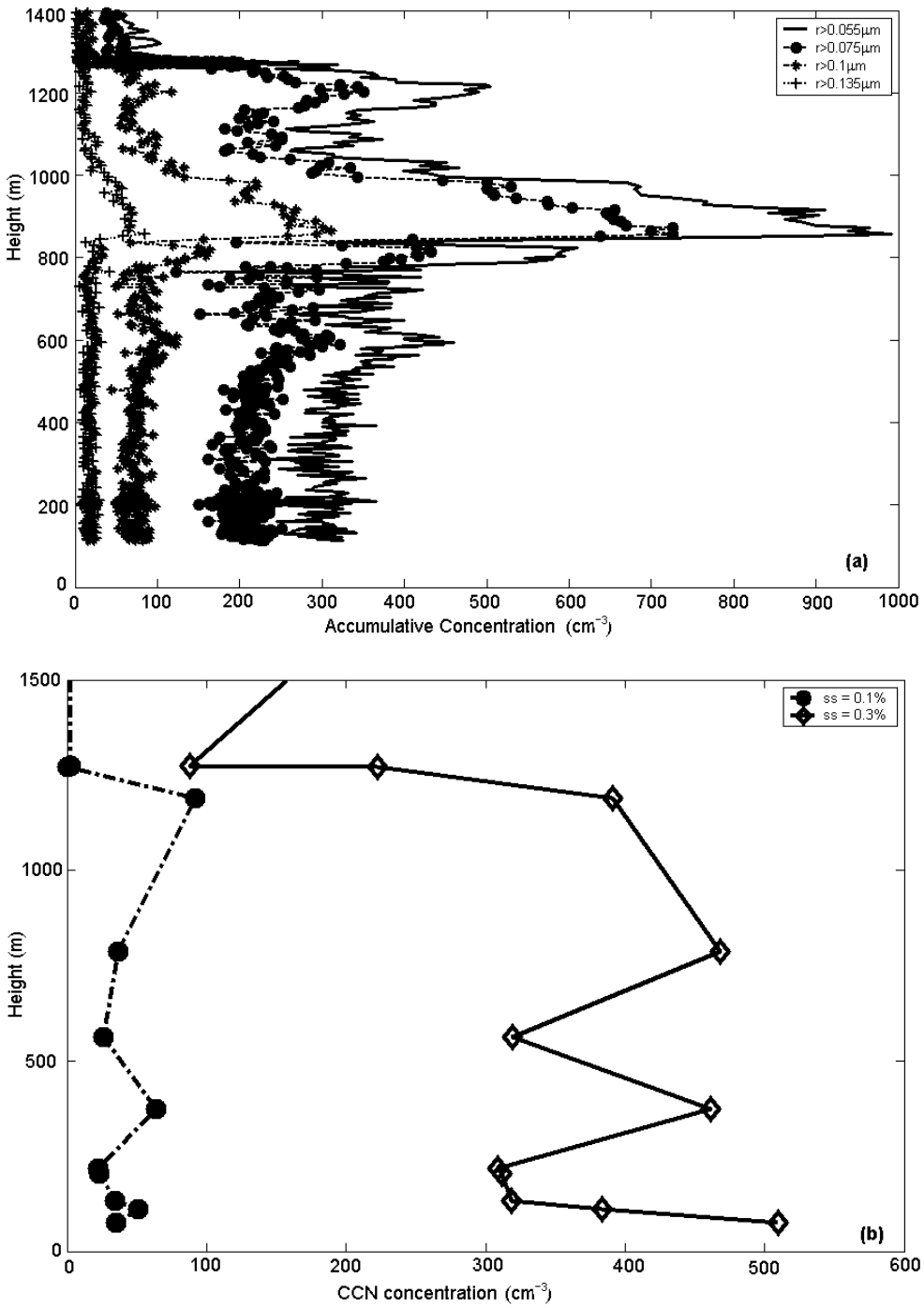

Fig. 2. ASASP and CCN data of 21 April 2001. (a) Profiles of ASASP accumulative particle number concentrations; (b) profiles of CCN concentration at supersaturations of 0.3% and 0.1%.

with

$$R_1 = 0.0078\,, \quad \sigma_1 = 2.2\,, \quad n_{\rm t} = 500$$

$$R_2 = 0.046\,, \quad \sigma_2 = 2.3\,, \quad n_{\rm t} = 1500$$

where r is the particle radius (in μm), $N(r)$ is the particle number concentration (in cm^{-3}), R is the mean particle radius (in μm), and $\log\sigma_i$ is the measure of particle polydispersity.

The fitting results based on CCN data are used as the input of the initialsize distribution. Figure 1 shows

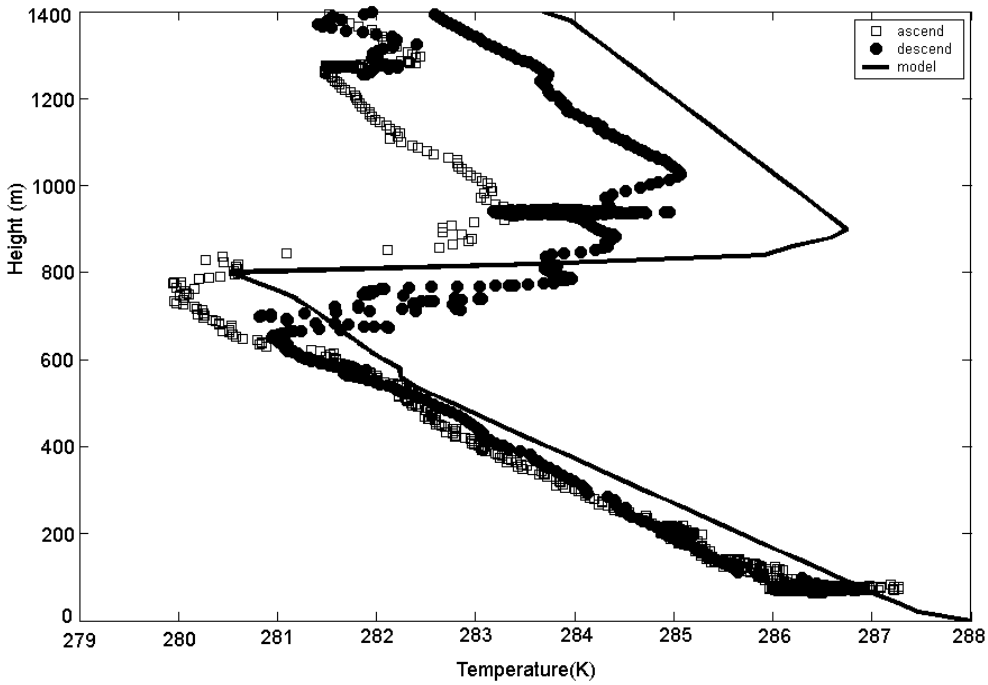

Fig. 3. Comparison between modeled temperature profile and aircraft measurements. Square marks are ascending aircraft data and circle marks are descending aircraft data. Solid line is the model results at 10 h.

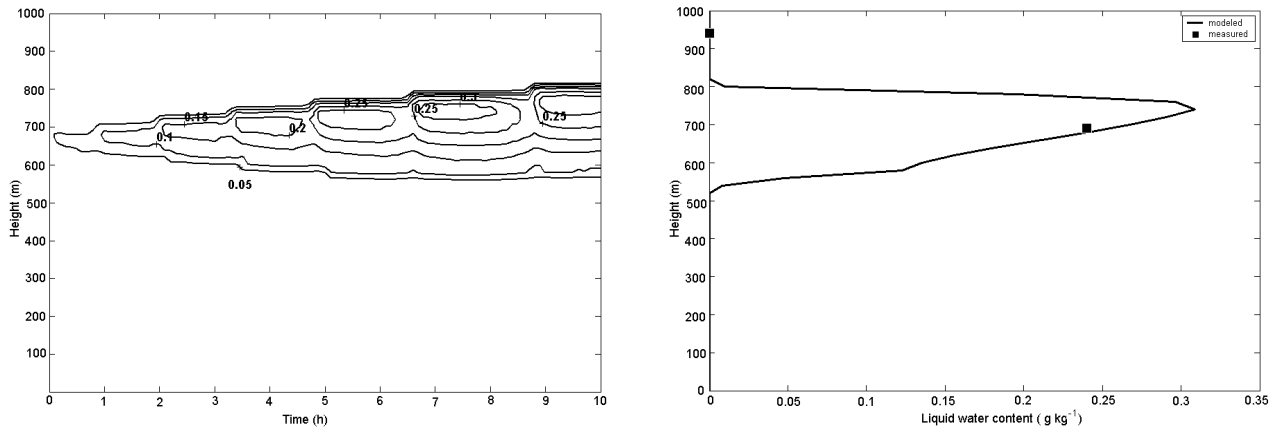

Fig. 4. Results of cloud liquid water content for the 0421 simulation. (a) Time evolution of the liquid water mixing ratio (in g kg^{-1}), and (b) modeled profile of the liquid water content and the measured data.

the initial size distribution for dry particles based on the fitting of CCN measurement data. We assume here that this aerosol particle size distribution exists homogeneously throughout the marine boundary layer.

6. Results and discussions

6.1 *Simulation of the 0421 case*

On 21 April 2001, an aircraft measurement was undertaken on the marine boundary layer clouds over the marine area south of Japan. Soundings of temperature and water mixing ratio profiles together with a roughly constant fine-particle profile of ASASP indicate a relatively well-mixed boundary layer around 800 m. The total water mixing ratio within the mixed layer is about 8.01 g kg^{-1}. During the sortie when the aircraft was able to profile to 80 m above the ocean surface in a cloudless area, the boundary-layer aerosol concentration of ASASP was of 500 cm^{-3} and CCN nconcentrations at 0.3% supersaturation were up to 500 cm^{-3}, identifying the region as a polluted air mass (Fig. 2). Observational data show no drizzle with the

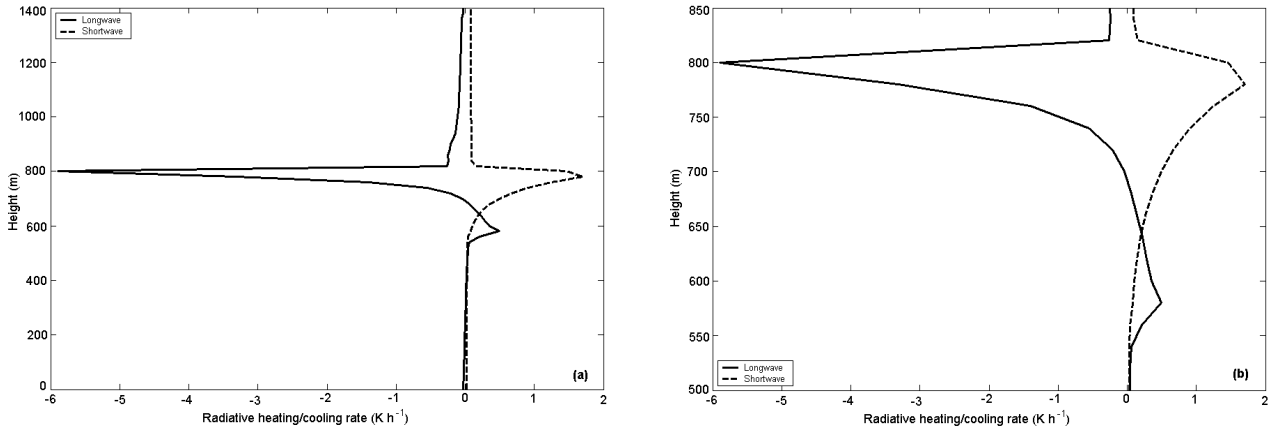

Fig. 5. Modeled profile of net radiative heating/cooling rate of longwave and shortwave radiation (in K h^{-1}). Panel (b) is an enlargement of the plot in panel (a).

cloud on this day. In general, the cloud for 21 April was a thin deck with the cloud top around 800 m without drizzle process. The simulation is referred to as "the 0421 case" experiment.

Figure 3 is the comparison between the modeled temperature profile and aircraft measurements. Square marks are the ascending aircraft data and circle marks are the descending aircraft data. The temperature profiles measured on 21 April 2001 illustrate an adiabatic subcloud layer topped by a thin cloud with a strong inversion above. The modeled temperature profile matches the measured profile through most of the depth of the boundary layer. There is a 100 m inversion layer located above 800 m containing a temperature step of about 6.1 K.

The evolution of the cloud layer and the comparison of the cloud liquid water content profile with the aircraft measurement are shown in Fig. 4b. After 10 hours of simulation, the model produces a cloud layer 300 m deep that caps the boundary layer which is 500 m deep. There was only one flight within the cloud of about 690 m on 21 April 2001. Because the one-dimensional model represents the averaging over the horizontal for the mean values, the measured cloud water content appearing in Fig. 4b is that averaged at the same level. The peak measurement data for cloud liquid water content is 0.59 g kg^{-1}. It is seen that there is generally good agreement between the calculated values and the aircraft measurement data. The modeled profile of cloud liquid water content at 10 h (Fig. 4b) peaks at the cloud top where it has a value of 0.32 g kg^{-1}.

Figure 4a shows the evolution of cloud liquid water content for the 0421 simulation. Cloud water content contours are shown at every 0.05 g kg^{-1}. The maximum water content shown is 0.32 g kg^{-1}. A maximum buoyancy flux in the cloud layer and water flux increases linearly from the surface to the cloud top. As discussed in Moeng et al. (1996), the fluxes of conserved variables are expected to be approximately linear between the surface value and cloud-top values that are determined by entrainment and radiative flux divergence. Unfortunately, there were few data for turbulence during the 2001 APEX/ACE-Asia field measurements. Although the model may produce a huge dataset for turbulent correlations, they cannot be compared with the measurements directly.

The profile of the net radiative heating/cooling rate is shown in Fig. 5. A net radiative cooling of 6 K h^{-1} is concentrated in the upper 100 m of the cloud while solar radiative heating almost crosses the cloud. There is a marked maximum of heating of about 0.4 K h^{-1} by longwave radiation just above the cloud base (Fig. 5b). Longwave radiative cooling occurring near the cloud top results in an increasingly unstable lapse rate near the cloud top. Net radiative cooling at the cloud top drives mixing by destabilizing the cloud layer itself and also by destabilizing the cloud layer with respect to the subcloud layer.

Figure 6 illustrates the evolutions of cloud drop size distributions at different levels. One striking property for the cloud drop size distributions is that in each layer the maxima of the curves are at almost the same location of 10 μm. Because the growth of the larger drops is retarded more than that of the smaller one, the droplet spectrum tends to become narrow as the cloud matures if condensation is the dominant process in the cloud. The size distributions of cloud drops at the cloud top are a little bit different with those of the other levels. There are more, small cloud drops at the upper cloud. As we discussed above, the cloud top temperatures decrease since the majority of the long-

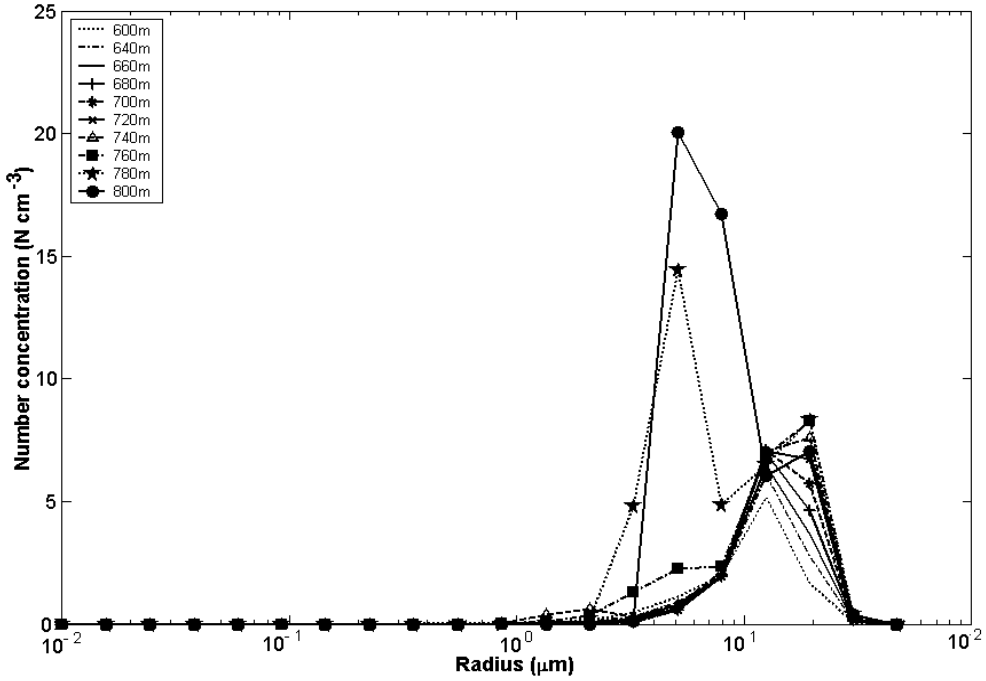

Fig. 6. Cloud drop size distributions at different levels at 10 h of the 0421 case.

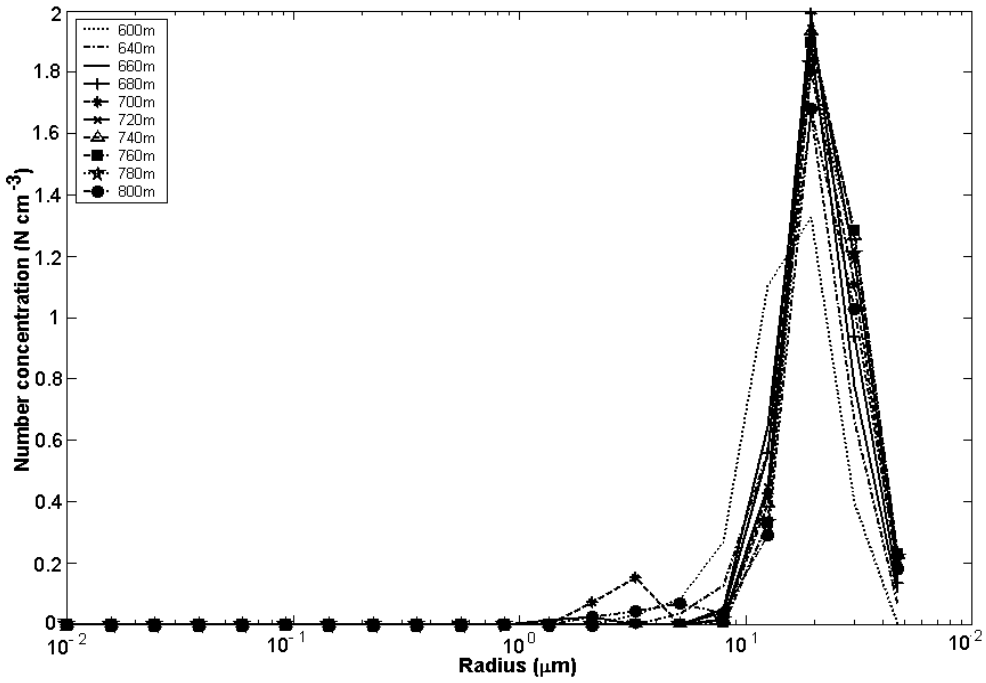

Fig. 7. Cloud drop size distributions at different levels at 10 h of the clean case.

wave radiation cooling takes place within the cloud top and there is a maximum upward water vapor flux due to turbulent transport. These processes enhance the supersaturation in the upper areas of the cloud. Then more CN are activated into small cloud drops thereafter undergoing the condensation process.

In summary, we have demonstrated here that the model we present in this paper simulates the marine stratocumulus fields in a reasonable manner compared with the available aircraft measurements.

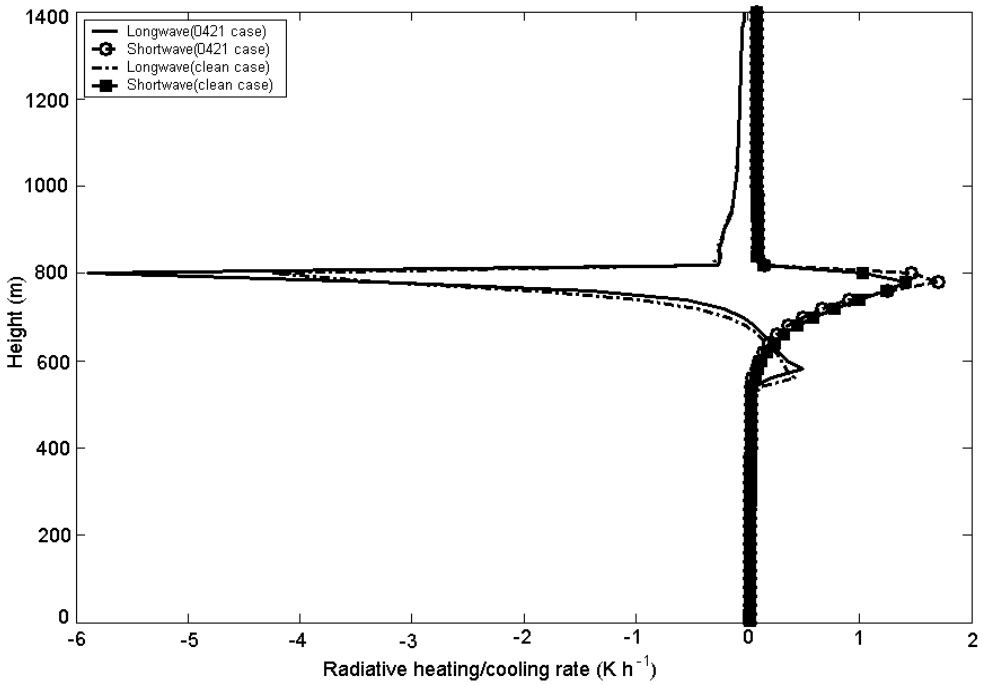

Fig. 8. Comparison of the radiation heating rates between the 0421 case and the clean case.

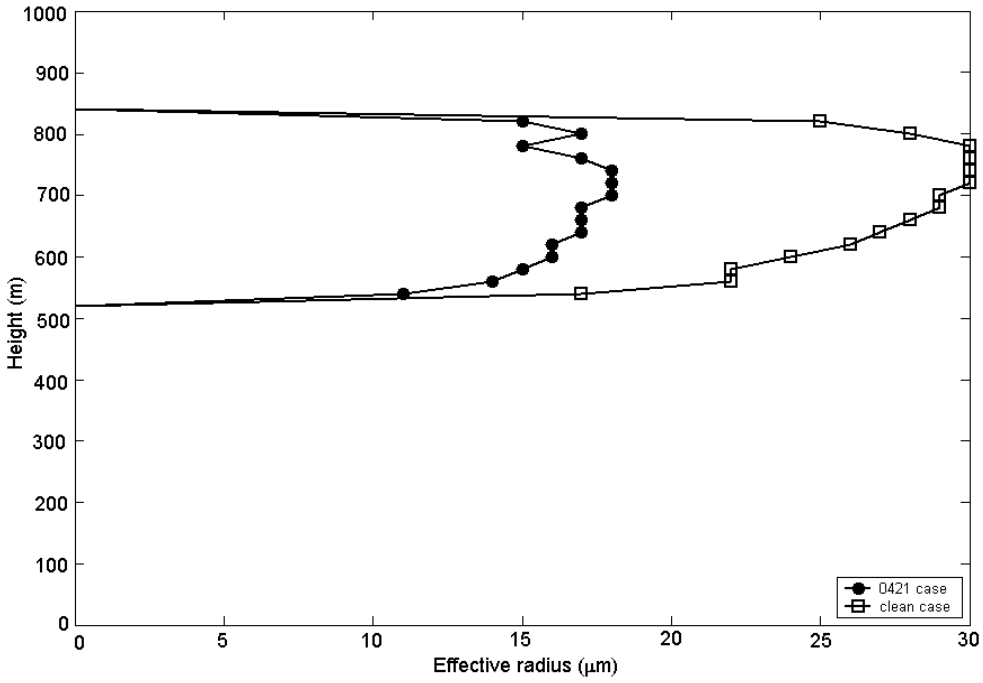

Fig. 9. Comparison of effective radius profiles between the 0421 case and the clean case.

6.2 *The role of initial CCN concentration*

There are a huge number of parameters in the models of thermodynamics, dynamics, radiation, and microphysics. One could conceivably run sensitivity tests to validate and evaluate the model by camparing the response of the model with certain kinds of observational data. Such kinds of work was done by Chen and Cotton (1985) and Ackerman (1995).

In this paper, we do not intend to repeat such sen-

sitivity studies for our model. One of the goals of this paper is to examine the role of initial CCN concentrations on the evolutions of Syratocumulus-Topped Boundary Layer (STBL) with the aircraft CCN data. The CCN data collected by a new CCN counter can provide the information of CCN size distributions. As discussed above, the 0421 case which we simulated was a polluted case. One more simulation is performed to examine the model response to a typical marine clean case. The shape of initial particle size distribution is determined by the parameters derived by lognormal fitting according to the observational data. The experiment is referred as the "clean case" experiment.

Model results for this case are compared with the 0421 case. The total kinetic energy (TKE) and liquid water content (LWC) do not differ significantly. The maximum difference between the LWC of these two cases is 0.1 g kg^{-1} around the upper cloud regions; for TKE the difference is 0.05 m^2 s^{-2}. A summary of the difference of these two cases is given in Table1. Changes of total liquid water content, its maximum, and the total TKE are modest. But there is a significant change for total cloud number concentration and the effective radius.

Figure 7 shows size distributions of cloud drops at different heights for the clean case. Compared with the 0421 case (Fig. 6), there are two striking properties shown in the model results for the cloud microphysics. One is that the cloud drop number concentration of the 0421 case are much higher than those of the clean case. The total number concentration of drops in a cloud is determined primarily by the concentration of CCN (e.g., Twomey, 1977). The other one is that the dry CN of the clean case grow into larger cloud drops than those of the polluted 0421 case. The droplet radii of the peak number concentration are on the order of 10 μm, i.e., approximately 10% larger than in the 0421 case.

Radiation within the cloud is significantly changed due to different initial CCN concentrations. Figure 8 shows the radiative cooling/heating rates of the two cases. Both the longwave radiation cooling rate and the shortwave heating rate are changed due to the change of initial CCN concentration. It can be seen that the decrease of the longwave cooling rate at the cloud top is up to 1.8 K h^{-1}, and the shortwave heating within the upper cloud region is also decreased.

In order to better understand the potential impacts of initial CCN concentration on the radiation, a comparison of effective radius is shown in Fig. 9. Effective radius is one of the most important cloud microphysical parameters used both in cloud radiation models and in the interpretation of satellite measurements. As is to be expected, effective radii are much larger in the clean case run with low initial CCN concentration than in the 0421 case. Twomey (1976) examined the dependence of cloud shortwave properties on the drop size distribution, and showed that as the mean drop radius is increased at a constant liquid water content, there is a small increase in the absorption and a larger increase in the transmission of the cloud. Clouds growing in a "clean" maritime airmass tend to have larger drops than polluted clouds of the same liquid water content and this therefore leads to a significantly larger absorption by the cloud-surface system.

Although the model can represent the general features of the stratocumulus-topped boundary layer, there are fundamental shortcomings in one-dimensional models (Brown, 1997; Bott et al., 1997; Stevens et al., 1998). However, long-term studies of the evolutions of cloud microstructure are not yet possible with multi-dimensional or LES models. A one-dimensional model with detailed cloud microphysics is still an attractive tool for studying the interactions between dynamics, cloud physics, and radiation processes. Therefore, more efforts should be focused on improving the parameterizations, formulations, and numerical modeling methods for the one-dimensional models. The new coupling method between cloud microphysics and dynamics presented in this model is just one of these efforts.

7. Summary and conclusions

In this paper, a one-dimensional 3rd-order turbulence closure model with size-resolved microphysics and radiative transfer has been developed for investigating aerosol and cloud interactions of the stratocumulus-topped marine boundary layer. A new method is presented for the coupling between the dynamical model and the microphysical model. This scheme allows the liquid water related correlations to be directly calculated rather than parameterized.

The new CCN counter can provide the CCN size distribution information rather than total CCN number concentration as the traditional CCN counters do at a certain supersaturation. A lognormal form is fitted based on the observed CCN data as the initialization for the model. This enables us to investigate the effect of different concentrations of CCN on dynamics and cloud microphysics.

A marine stratocumulus case observed during the 2001 APEX/ACE-Asia field measurements was selected to be simulated by the model we present here. The model results show that the general features of the stratocumulus-topped marine boundary layer predicted by the model are in agreement with the measurements. The comparison between the model results

Table 1. Summary of 0421 case and the clean case.

Variables		0421 case	Clean case
Cloud top properties	LWC (g kg^{-1})	0.20	0.13
	Nc (cm^{-3})	40.2	2.7
	Temperature (K)	280.54	280.42
	Re (μm)	16	28
Bulk cloud properties	Total Nc (cm^{-3})	260.85	45.09
	Total LWC (g kg^{-1})	2.57	2.39
	Max. LWC/level (m)	0.32/780	0.27/760
	Total TKE (m s^{-2})	5.15	4.88

and aircraft measurements is quite consistent. Although there are some limitations and shortcomings in one-dimensional cloud modeling, the present study suggests that the one-dimensional model with explicit microphysics and a detailed radiation scheme can be used as a powerful tool for research into the cloudy boundary layer. Of course it would be even better to test and validate the model using turbulence measurements through a cloud layer during field experiments.

The model responses to a different CCN initial concentration are examined. Numerical results are consistent with both observations and expectations. In the clean marine case, cloud drop concentrations decrease, their effective radii increase significantly, and cloud liquid water content decreases compared with the polluted 0421 case. Initial CCN loadings have large impacts on the evolution of cloud microstructure and radiation transfer, while they have a modest effect on thermodynamics. The cloud micro properties are strongly modified by the different CCN concentrations. This modification is expressed by the far different cloud drop concentrations and the different locations of peak number concentrations in the size distribution. Increased CCN concentration leads to a significant decrease of cloud effective radius.

Acknowledgments. This research was supported by the National Natural Science Foundation of China (NSFC) under Grant No. 40005001 and the key laboratory of storm and disaster of Educational Department of China. The authors are grateful to Prof. T. Nakajima from the University of Tokyo for discussions. The coupling method used in this paper was initially investigated by Prof. Qing Wang from US Naval Postgraduate School. We thank Dr. Shouping Wang from NASA for his one-dimensional high-order turbulence closure model. The data used here are rom APEX of Japan.

REFERENCES

Ackerman, A. S., P. V. Hobbs, and O. B. Toon, 1995: A model for particle microphysics, turbulent mixing, and radiative transfer in the stratocumulus-topped marine boundary layer and comparisons with measurements. *J. Atmos. Sci.*, **52**, 1204–1236.

Barkstorm, B. R., 1978: Some effects of 8–12 μm radiant energy transfer on the mass and heat budgets of cloud droplets. *J. Atmos. Sci.*, **35**, 665–673.

Bechtold, P., and coauthors, 1996: Modeling a stratocumulus-topped PBL: Intercomparison among different one-dimensional codes and with large eddy simulation. *Bull. Amer. Meteor. Soc.*, **77**, 2033–2042.

Bott, A., 1998: A numerical model of the cloud-topped planetary boundary layer: Radiative forcing of aerosols in stratiform clouds. *Ecological Modeling*, **113**, 13–30.

Bott, A., 1999: A numerical model of the cloud-topped planetary boundary layer: Chemistry in marine stratus and the effects on aerosol particles. *Atmos. Environ.*, **33**, 1921–1936.

Bott, A., and coauthors, 1996: A numerical model of the cloud-topped planetary boundary layer: Radiation, turbulence and spectral microphysics in marine stratus. *Quart. J. Roy. Meteor. Soc.*, **122**, 635–667.

Bott, A., and coauthors, 1997: Reply to a comment by R. Brown on 'A numerical model for the cloud-topped planetary boundary layer: Radiation, turbulence and spectral microphysics in marine stratus'. *Quart. J. Roy. Meteor. Soc.*, **123**, 1785–1787.

Bougeault, Ph., 1981a: Modeling the trade-wind cumulus boundary layer. Part I: Testing the ensemble cloud relations against numerical data. *J. Atmos. Sci.*, **38**, 2414–2428.

Bougeault, Ph., 1981b: Modeling the trade-wind cumulus boundary layer. Part II: A high-order one-dimensional model. *J. Atmos. Sci.*, **38**, 2429–2439.

Bougeault, Ph., 1985: The diurnal cycle of the marine stratocumulus layer: A higher-order model study. *J. Atmos. Sci.*, **42,** 2826–2843.

Brown, R., 1997: Comment on "A numerical model of the cloud-topped planetary boundary layer: Radiation, turbulence and spectral microphysics in marine stratus." by A. Bott, Trautmann, T., Zdunkowski, and W., *Quart. J. Roy. Meteor. Soc.*, **123**, 1783–1784.

Buck, A. L., 1981: New equations for computing vapor pressure and enhancement factor. *J. Appl. Meteor.*, **20**, 1527–1532.

Chen, C., and W. R. Cotton, 1987: The physics of the marine stratocumulus-topped mixed layer. *J. Atmos. Sci.*, **44**, 2951–2977.

Duynkerke, P. G., and A. Driedonks, 1987: A model for the turbulent structure of the stratocumulus-topped

atmospheric boundary layer. *J. Atmos. Sci.*, **44**, 43–64.

Duynkerke, P. G., and A. Driedonks, 1988: Turbulent structure of a shear-driven stratus-topped atmospheric boundary layer: A comparison of model results with observations. *J. Atmos. Sci.*, **45**, 2343–2351.

Ding, S. G., 2001: The impacts of radiation transfer on cumulus processes. M. S. thesis, Peking University, 109pp.

Feingold, G., W. R. Cotton, B. Stevens, and A. S Frisch, 1996: On the relationship between drop in-cloud residence time and drizzle production in numerically simulated stratocumulus clouds. *J. Atmos. Sci.*, **53**, 1108–1122.

Feingold, G., and coauthors, 1998: Simulations of marine stratocumulus using a new microphysical parameterization scheme. *Atmos. Res.*, 47–48, 505–528.

Hall, W. D., 1980: A detailed microphysical model within a two-dimensional dynamic framework: Model description and preliminary results. *J. Atmos. Sci.*, **37**, 2486–2507.

Lilly, D. K., 1968: Models of cloud-topped mixed layers under a strong inversion. *Quart. J. Roy. Meteoro. Soc.*, **94**, 292–309.

Liou, K. N., and coauthors, 1998: A simple formulation of the delta-four-stream approximation for radiative transfer parameterizations. *J. Atmos. Sci.*, **45**, 1940–1947.

Liou, K. N., 1992: *Radiation and Cloud Processes in the Atmosphere*. Oxford University Press, 487pp.

Mellor, G. L., 1977: The Gaussian cloud model relations. *J. Atmos. Sci.*, **34**, 358–365.

Moeng, C.-H., 1986: Large-eddy simulation of a stratus-topped boundary layer. Part I: Structure and budgets. *J. Atmos. Sci.*, **43**, 2886–2990.

Moeng, C.-H., and coauthors, 1996: Simulation of a stratocumulus-topped PBL: Intercomparison among different numerical codes. *Bull. Amer. Meteor. Soc.*, **77**, 261–278.

Nicholls, S., 1984: The dynamics of stratocumulus: Aircraft observations and comparisons with a mixed layer model. *Quart. J. Roy. Meteor. Soc.*, **110**, 783–820.

NOAA/NASA, 1976: US Standard Atmosphere.

Pruppacher, H. R., and J. D. Klett, 1997: *Microphysics of Clouds and Precipitation*. Kluwer Academic Publishers, 955pp.

Randall, D. A., and coauthors, 1984: Outlook for research on subtropical marine stratiform clouds. *Bull. Amer. Meteor. Soc.*, **65**, 1290–1301.

Seinfeld J., and S. N. Pandis, 1998: Atmospheric Chemistry and Physics. A Wiley-Interscience Publication.

Stevens, and coauthors, 1998: A critique of one- and two-dimensional models of boundary layer clouds with binned representations of drop microphysics. *Atmos. Research*, 47–48, 529–553.

Slingo, A., and coauthors, 1982: Aircraft observations of marine stratocumulus during JASIN. *Quart. J. Roy. Meteor. Soc.*, **108**, 833–856.

Sommeria, G., and J. W. Deardorff, 1977: Subgrid-scale condensation in models of nonprecipitating clouds. *J. Atmos. Sci.*, **34**, 344–355.

Taylor, J. P., and A. S. Ackerman, 1999: A case-study of pronounced perturbations to cloud properties and boundary-layer dynamics due to aerosol emissions. *Quart. J. Roy. Meteor. Soc.*, **125**, 2643–2661.

Twomey, S., 1974: Pollution and the planetary albedo. *Atmos. Environ.*, **8**, 1251–1256.

Twomey, S., 1977: *Atmospheric Aerosols*. in Elsevier, 251pp.

Twomey, S., 1976: The effects of fluctuations in liquid water content on the evolution of large drops by coalescence. *J. Atmos. Sci.*, **33**, 720–723.

Twomey, S., and coauthors, 1984: An assessment of the impact of pollution on global cloud albedo. *Tellus*, **36**, 356–366.

Wang, S., and Q. Wang, 1994: Roles of drizzle in a one-dimensional third-order turbulence closure model of the nocturnal stratus-topped marine boundary layer. *J. Atmos. Sci.*, **51**(11), 1559–1576.

Zhao, C. S., and coauthors, 1996: The production and evolution of atmospheric aerosols in remote marine boundary layer. Ph. D. dissertation, Peking University.

Zhao, C. S., 1998: Numerical modeling of the production and evolution of atmospheric aerosols in marine boundary layer. *Progress in Natural Science*, **8**(4), 440–448.